MAGNETORESISTANCE

Perovskite materials continue to be focal points for materials research and development efforts around the world. Perovskites such as barium titanate were extensively studied and used in the 1940s as active elements in communications systems. More recently, the confluence of novel thin film deposition techniques and the observation of superconductivity at temperatures above that of liquid nitrogen have triggered a flurry of activity in a broad class of perovskite and related materials. Another parallel area of considerable technological and scientific interest is ferroelectric and dielectric perovskites. Thin films of these materials, integrated on Si/GaAs, are strong candidates for solid-state memories, sensors, actuators, monolithic microwave elements, infrared sensors, and so on. Focusing specifically on the magnetic perovskites, considerable work has already been carried out on magnetic perovskites based on Fe, Co, Ni, and Mn. A very detailed review of the structural chemistry, magnetism, and transport in these systems is available in a review by Goodenough (1). We begin this review by summarizing some of the initial results that have led to the "rebirth" of this field. Because manganese-based rare earth perovskites with the typical chemical formulation of $La_{1-x}M_xMnO_{3\pm y}$ (where M is a divalent Group II cation such as Ca, Sr, Ba) exhibit the most interesting magnetotransport effects, we focus specifically on this family of compounds. Figure 1 schematically illustrates the crystal structure of this perovskite phase. What is noteworthy is that very rarely do these compounds adhere to the basic cubic perovskite structure; a variety of structural distortions are possible and have been observed as a function of composition and processing. Almost simultaneously, Chahara et al. (2) and Von Helmholt et al. (3) presented results of large magnetoresistance in epitaxial thin films of two of the prototypical compounds within this family. Almost immediately afterward, two different groups, one led by Jin et al. (4) and the other from this laboratory (5), published data showing magnetoresistance values much higher than that published by the two original papers. Figure 2 shows one typical plot of the resistance as a function of magnetic field; the colossal magnetore-

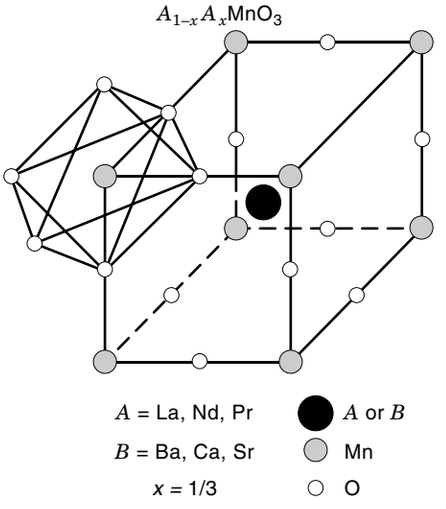

Figure 1. A schematic of the perovskite crystal structure of substituted rare earth manganites.

sistance (CMR) value in this case was much larger than 10^5% at a temperature of 77 K and a magnetic field of 5 T. Note that this value of MR is larger than 100% because it is defined as $(R_0 - R_H)/R_H$, where R_0 is the resistance at zero field and R_H is the value in an applied field of H. When one puts this into a technological perspective, the field values needed to get useful MR are much too high. In many research programs, this was the trigger point that led to detailed studies of various factors that have an impact on the temperature and field dependence of magnetoresistance. Among them, the effect of lattice strain, oxygen stoichiometry, and the effects of layering and heterostructuring are being studied. The thin films and heterostructures are typically deposited by pulsed laser deposition. Refer to one of the many articles in current literature for a detailed description of the thin film processing procedures as well as the details of the various experimental techniques that are being employed to characterize the materials.

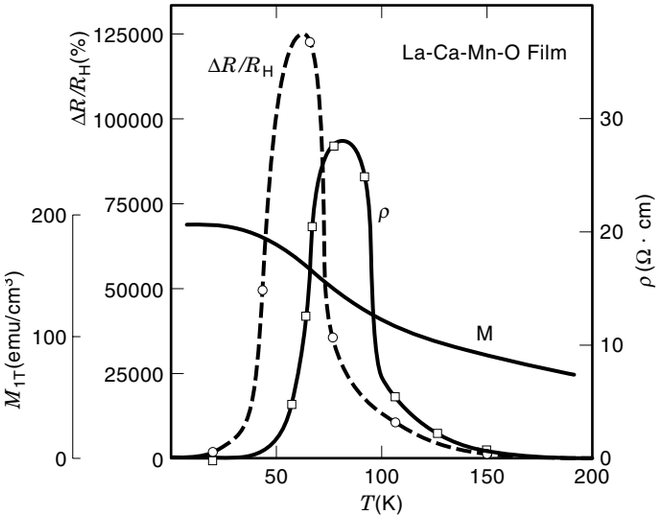

Figure 2. Temperature dependence of saturation magnetization, resistivity, and magnetoresistance for an epitaxial La–Ca–Mn–O film.

Perovskite materials, even in the bulk, are very susceptible to lattice distortions, which may occur either spontaneously (e.g., ferroelectrics) or as a consequence of process-induced variations of, for example, the oxygen stoichiometry. When grown in thin film form, they are even more susceptible to lattice strains, especially when constrained by heteroepitaxy to the substrate lattice. For example, the bulk lattice parameter of $La_{0.7}Sr_{0.3}MnO_3$ (LBMO) is 3.88 Å whereas that of one common single crystal oxide substrate $LaAlO_3$ (LAO) is 3.79 Å, leading to a 2.4% compressive strain in the plane of the film (6). On the other hand, if the same material is grown on $SrTiO_3$ (STO), the lattice mismatch is smaller (1.0%) and is tensile. This leads to out-of-plane strains in the film, as illustrated in Fig. 3 where we see that 1000 Å thick films grown on these two types of surfaces show different out-of-plane lattice parameters. What is interesting to note is that, in both cases, the films do not seem to have relaxed into their bulk lattice dimensions, even after growth of 1000 Å. Because these materials do not have any other source of magnetic anisotropy, they strongly exhibit stress (or conversely strain) induced magnetic anisotropy. For example, in the absence of any magnetocrystalline anisotropy, one would expect the easy direction of magnetization to be controlled by the magnetostatic energy, thereby inducing an in-plane easy magnetization direction (or easy magnetization plane). This is indeed seen in magnetic hysteresis, measured in the plane of the film, of the films grown on STO, Fig. 4. However, the films grown on LAO are actually preferentially magnetized out of the plane (see Fig. 4), with the magnetization vector possibly lying at an angle to the substrate surface. Furthermore, this conclusion is authenticated by magnetic force microscopy (MFM) studies of the film surface, which are illustrated in Fig. 5. The films grown on STO show a "feathery" surface structure (reflecting the fact that there is no magnetization vector normal to the film surface), whereas the films on LAO show the characteristic maze domain structure typical of uniaxial materials. Is this a possible ingredient in obtaining large MR values? The magnetotransport measurements do not indicate dramatic differences in MR values for these two types of films. Figure 6 shows MR as a function of applied magnetic field for the films on STO and LAO, and although there is a small increase in MR for the films on STO, it is not dramatic.

Several approaches to reduce or eliminate this lattice strain are currently being studied. Among them, it has been found that changing the thickness of the film during deposition can progressively relax the mismatch strain, as illustrated through the X-ray diffraction spectra in Fig. 7. The progressive decrease in the c-axis lattice parameter can be interpreted as a consequence of a reduction in the compressive in-plane stresses that lead to an increase in the c-axis lattice parameter in the first place. It is worth noting that this does not lead to a completely relaxed film. Annealing a 1000 Å thick film in oxygen at 900°C also produces some partial relaxation, but the c-axis lattice parameter is still larger than the bulk value, as shown in Fig. 8. However, this does have a significant effect on the magnetic hysteresis loops. Figure 9 compares hysteresis loops for the same sample, before and after the oxygen annealing. The initial susceptibility has increased by almost an order of magnitude with an almost

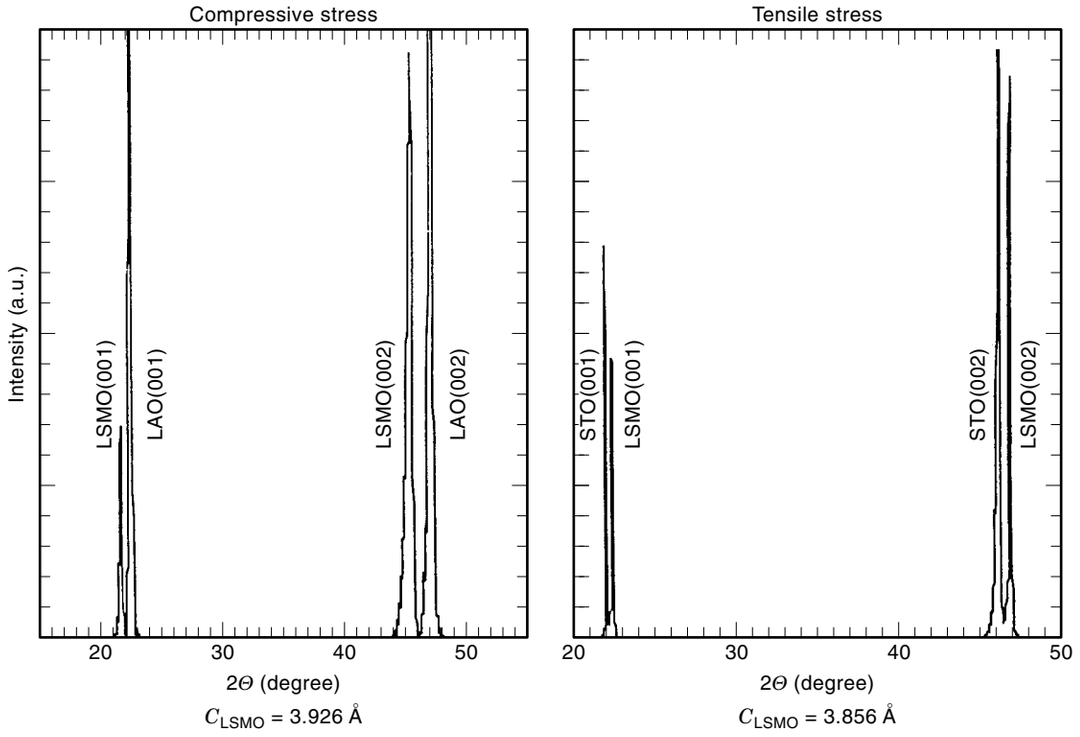

Figure 3. X-ray Bragg scans from epitaxial LSMO films grown on LAO and STO substrates illustrating the influence of substrate-film lattice mismatch on the film lattice parameters.

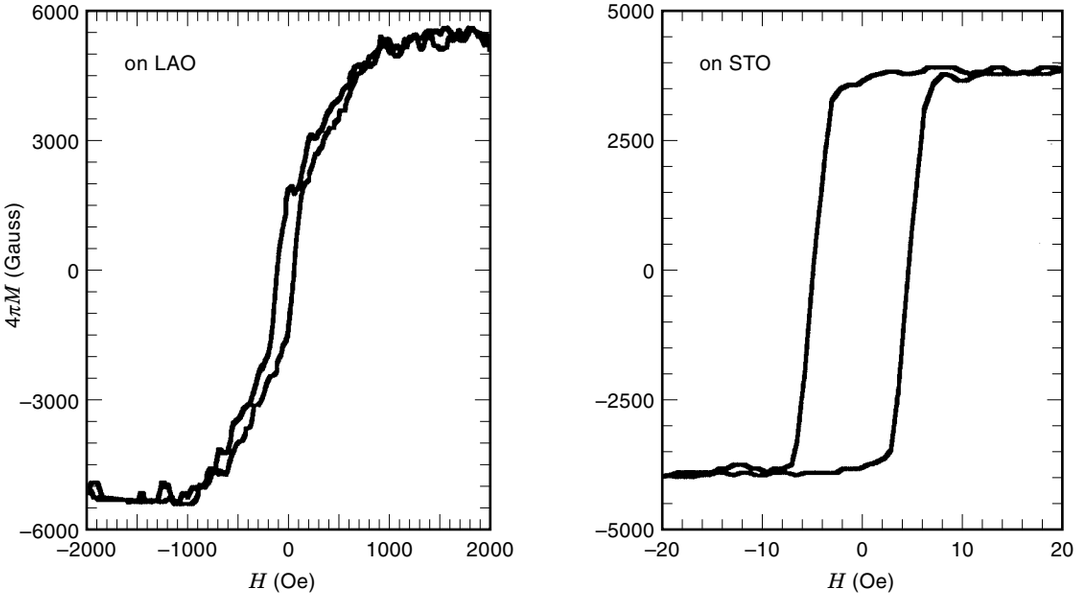

Figure 4. Room temperature, in-plane hysteresis loops from epitaxial LSMO films grown on LAO and STO substrates showing the influence of strain on the preferred magnetization direction.

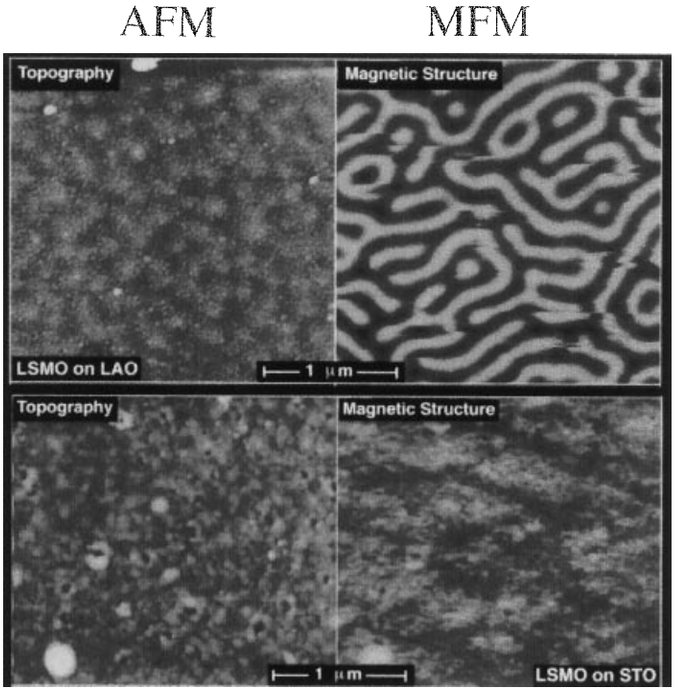

Figure 5. Magnetic force microscopy images of the film surface in the case of STO and LAO substrates illustrating the effect of mismatch strain on the preferred magnetization direction and consequently on the domain structure.

doubling of the saturation magnetization. Transmission electron microscopy of the as-grown samples indicate that the film has ordered domains with sizes in the range of 10 nm to 30 nm, as illustrated in the dark field micrograph in Fig. 10. This image was obtained using the superlattice reflection which is circled in the diffraction pattern shown in the inset. The regions in bright contrast correspond to one set of ordered domains, whereas the regions in dark contrast correspond to the other. We also observe that the domain size increases considerably with annealing in oxygen. The interfaces between these domains (i.e., the antiphase boundaries) can act as scattering sites during transport. The effect of these types of defects on the magnetotransport properties needs to be understood through further systematic experiments.

One of the most effective ways to alleviate the effects of lattice mismatch strain is to use buffer layers. A very suitable buffer layer is epitaxially grown $SrTiO_3$ on a [001] $LaAlO_3$ substrate. STO has a lattice parameter of 3.905 Å, almost

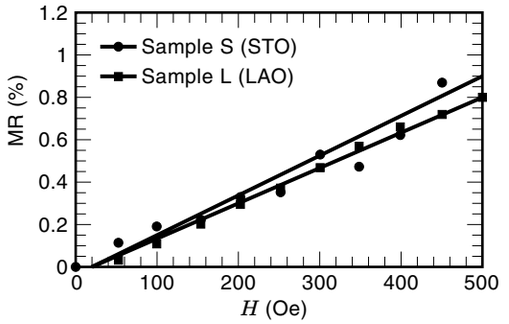

Figure 6. Magnetoresistance as a function of applied field for the epitaxial films grown on STO and LAO showing that the mismatch strain has only a minimal influence on the MR properties.

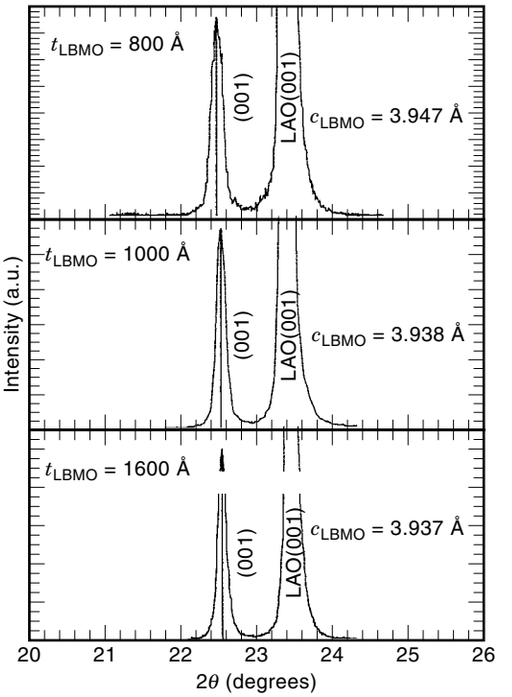

Figure 7. X-ray diffraction spectra as a function of thickness of the LSMO layer, showing the partial relaxation of lattice mismatch strain with increasing thickness.

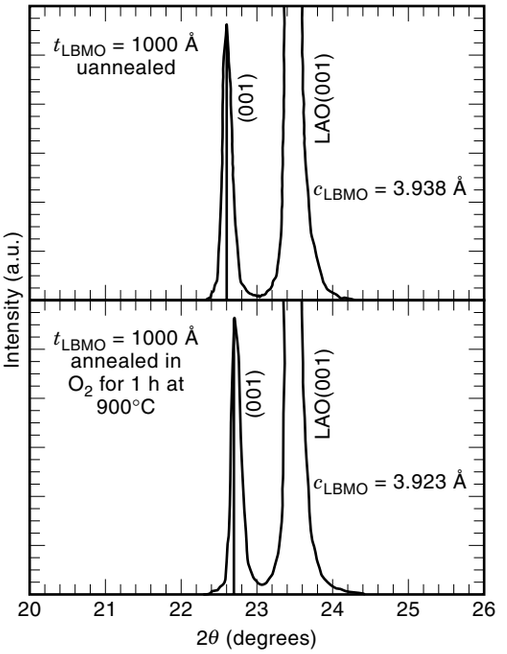

Figure 8. X-ray diffraction spectra of an epitaxial LSMO film before and after annealing at 900°C showing the reduction in the out-of-plane lattice parameter resulting from relaxation of the lattice mismatch strain.

identical to that of LBMO (3.9 Å). A thin layer (about 700 Å to 1000 Å) of STO is typically used as a buffer layer on which the LBMO layer is then grown. The X-ray diffraction patterns in Fig. 11 clearly show the effectiveness of the STO layer. The LBMO layer now has an out-of-plane lattice parameter of 3.907 Å, which is very close to the bulk value. As expected, this is also reflected in the magnetic properties, primarily the initial susceptibility and the saturation magnetization, which are shown in Fig. 12.

The obvious question now arises: is this sufficient to improve the MR properties of the CMR layer, especially at low fields? Direct current (dc) and microwave MR measurements

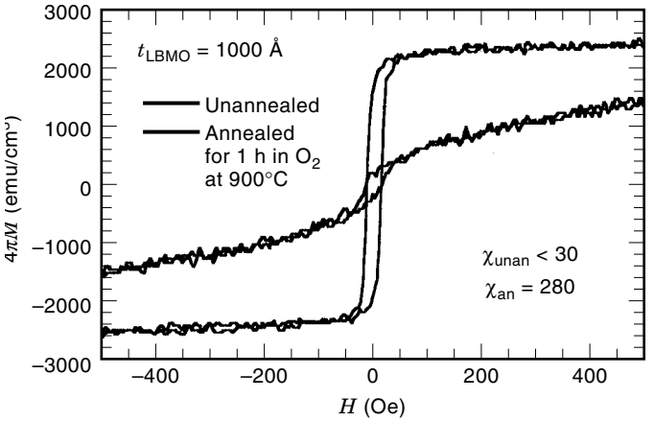

Figure 9. In-plane hysteresis loops of the LSMO film before and after annealing at 900°C showing the significant improvement in the squareness as well as the low-field susceptibility.

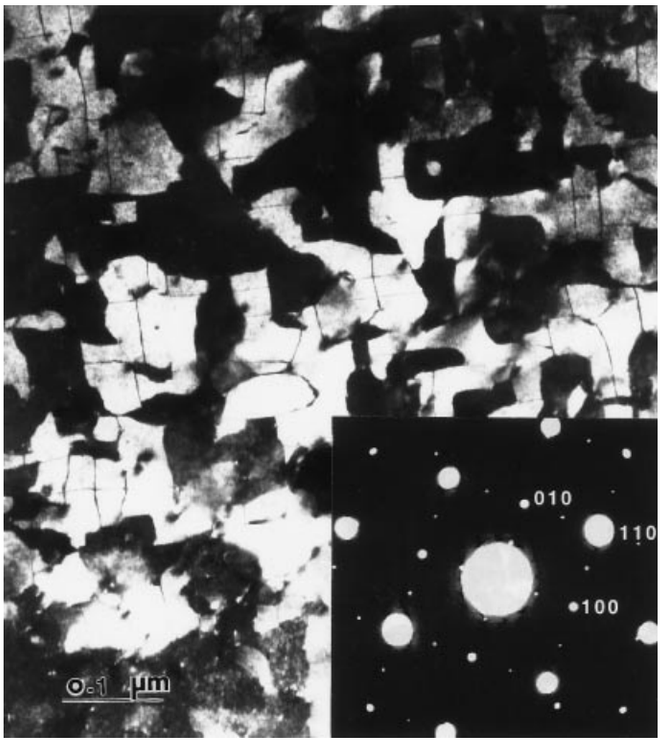

Figure 10. A dark-field transmission electron micrograph of the as-grown LCMO film showing the existence of ordered antiphase domain structure. The inset shows the electron diffraction pattern and the superlattice reflection that was used to form this dark-field image.

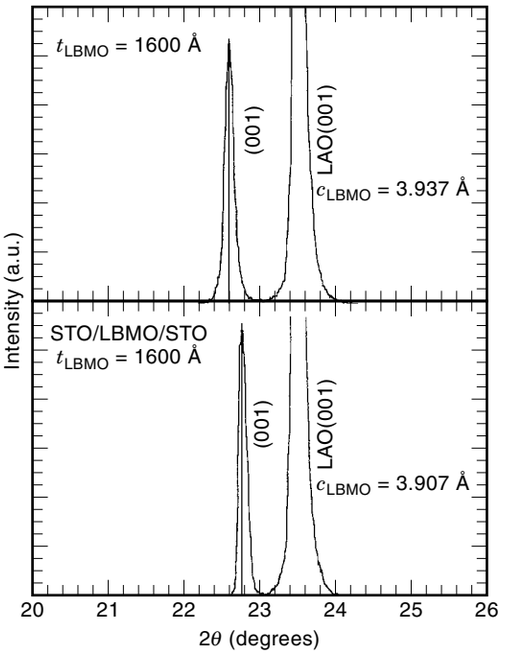

Figure 11. X-ray diffraction patterns from an epitaxial LBMO thin film grown on a [001] LAO substrate with and without a STO buffer layer, showing the beneficial effect of the STO layer in relaxing the mismatch strain.

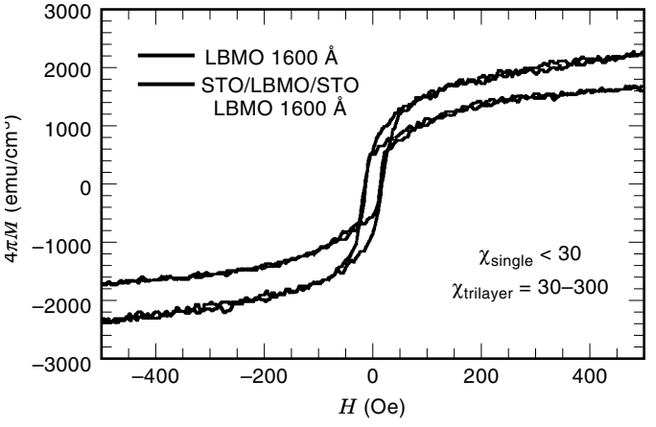

Figure 12. In-plane hysteresis loops of the LBMO film grown with and without the STO buffer layer, showing the strong enhancement of low-field susceptibility.

indicate that there is some improvement in the low-field MR values, but it is not significant enough to have an impact on an actual implementation in low-field sensing applications. Figure 13 compares the microwave and dc MR values, measured at 1800 Oe, and clearly demonstrates that there is very little difference between these two types of measurements. An interesting, but perhaps obvious, point that arises from this result is that the magnetotransport and the consequent MR effect are directly associated with the electronic properties of the manganite. Further supporting evidence for this is also available from optical measurements (7). It is also of interest to note that in these epitaxial films, the highest MR is obtained very close to the metal-insulator transition, although there is still considerable debate over the actual location of the peak in the MR value vis-à-vis the ferromagnetic Curie temperature (8). Contrast this with data that will be presented later on nonepitaxial films that show a very different MR behavior. Finally, note that at this field level, the MR values are still only of the order of a few percent, which is still not sufficient for low-field magnetic sensing applications

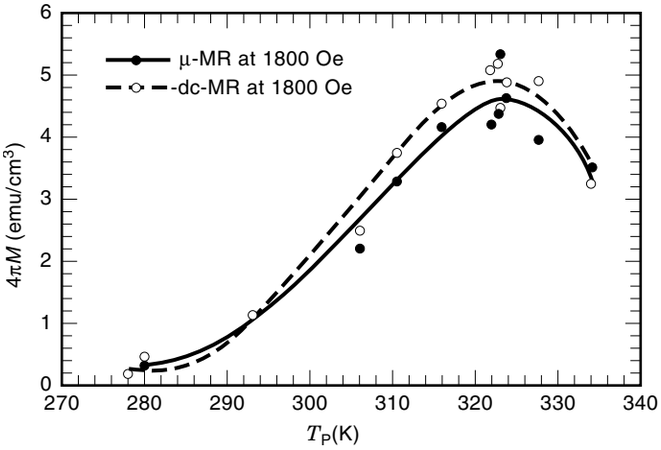

Figure 13. Comparison of the dc and microwave MR of an epitaxial LBMO film at an applied field of 1800 Oe, clearly demonstrating that the two types of measurements yield the same MR value.

such as in read heads. Obtaining large MR values at low fields clearly requires further ingenuity and engineering of the thin films and their microstructures.

Two different directions are currently being explored by many of the groups that are intensively involved in this field. Hwang et al. (9), Ju et al. (10), and Gupta et al. (11) made a very interesting observation that in polycrystalline CMR materials, the MR values actually increase as the temperature is progressively decreased below the peak resistance temperature. This is in direct contrast to the epitaxial films, which show the largest MR values very close to the peak resistance temperature and drop to very small values well below the ferromagnetic transition. This was the first evidence for magnetoresistance behavior that is distinctly different from the CMR effect and that is not closely associated with the metal-insulator transition. This effect is associated with the granularity of the system (either bulk or thin film) and has been described as a spin-polarized tunneling phenomenon. Interestingly enough, a similar effect was also observed in epitaxial LBMO/STO/LBMO heterostructures by Lu et al. (12) and Sun et al. (13), in which the STO tunnel barrier layer thickness was on the order of 50 Å. The authors have suggested that the STO layer behaves like a spin-polarized tunnel barrier. Although the detailed physics behind this is still being resolved, what has emerged is that there is another source of MR, associated with granularity or alternatively structural interfaces. Two important types of structural interfaces can be visualized, namely, natural interfaces such as grain boundaries and antiphase boundaries and those created artificially by heterostructuring. We discuss the structural aspects of these two types next and then conclude with some results and comments on the magnetotransport behavior across such interfaces.

Four distinct classes of films can be generated, based on the type of substrate structure, surface chemistry, and deposition conditions. For example, by systematically changing the nature of the substrate surface, we can obtain these four distinct microstructures. For example, a fully epitaxial film of the CMR material (e.g., LSMO) on an almost lattice matched substrate such as LAO or STO can be obtained, in which case there is full in-plane orientational locking (i.e., $[100]_{LSMO} \| [100]_{LAO}$). A highly *c*-axis oriented film is obtained with in-plane crystallographic grain boundaries using a substrate with a large lattice mismatch (e.g., MgO) and a suitable template layer [e.g., Y–Ba–Cu–O (YBCO)]. On a substrate such as SiO_2/Si with a thin layer of bismuth titanate as a structural template, highly *c*-axis out-of-plane oriented films with random in-plane grain boundaries are obtained. Finally, when there is no structural or chemical similarity between the film and the substrate, typically polycrystalline films result. Figure 14 shows representative examples of in-plane phi-scans of the first three types and illustrates the difference in in-plane structural coherence between them. On an LAO substrate [Fig. 14(a)], the observation of intensity maxima spaced 90° apart reflects the fourfold symmetry of the film in response to the same for the substrate and clearly reflects orientational locking. On the [001] MgO substrate with the YBCO layer, the YBCO layer grows highly *c*-axis oriented with in-plane grain boundaries which are dictated by specific geometrical relationships, also known as the coincidence site lattice (CSL) model (or in the case of YBCO on MgO, the near model (14). Figure 14(b) shows the phi-scan for this case and

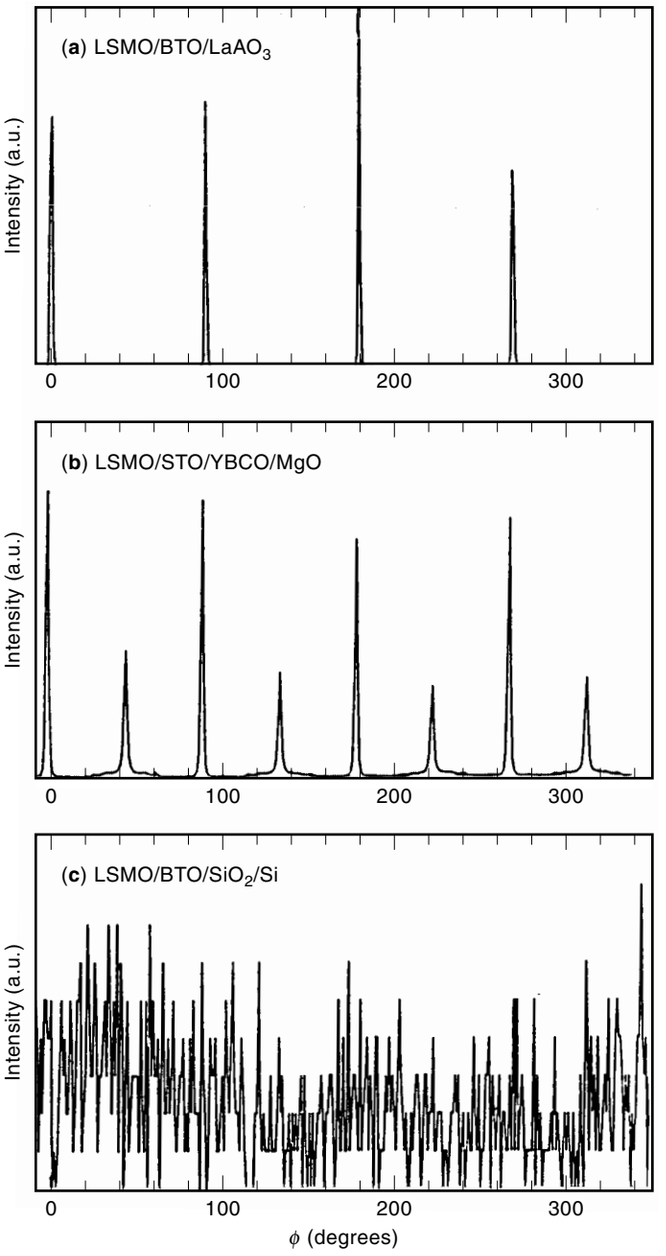

Figure 14. X-ray phi-scans from three types of films: *Top:* epitaxial film on LAO substrate showing the full in-plane orientation locking; *center:* highly [001] oriented film on MgO with a predominance of 45° in-plane grain boundaries; *bottom:* highly [001] oriented film on SiO_2/Si with no in-plane orientation locking.

clearly shows the presence of intensity maxima spaced 45° apart, indicating the existence of 45° rotation grain boundaries in the plane of the film. Indeed, these types of grain boundaries are observed in planar section TEM images, shown for example in Fig. 15. Figure 15(a) shows the actual image of this grain boundary, whereas Fig. 15(b) shows the same image after being digitally filtered. Figures 15(c) and (d) show light optical diffraction patterns obtained from the two grains showing that they are of a single orientation, whereas the composite optical diffractogram in Fig. 15(e) shows clearly

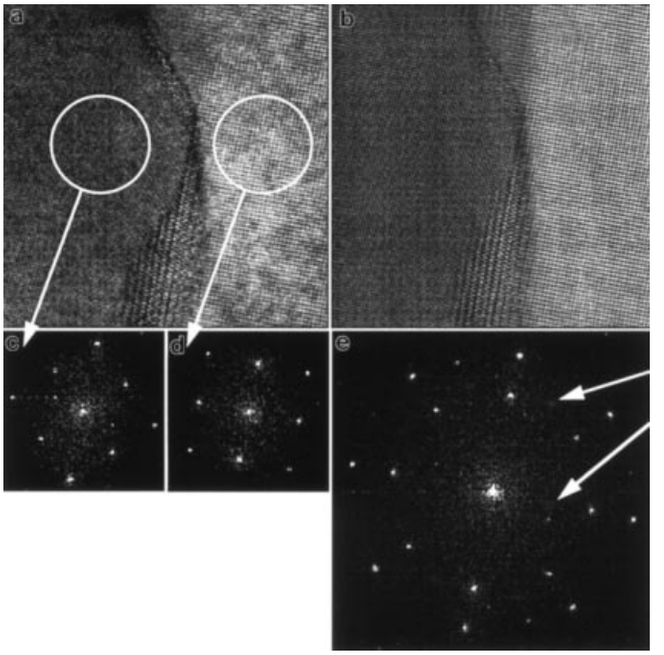

Figure 15. Planar section transmission electron micrographs of the film grown on MgO showing the characteristic 45° grain boundaries, identified from the optical diffraction patterns.

the 45° rotation between them. Returning to Fig. 14(c), this X-ray phi-scan shows the case of a LSMO film grown on BTO/SiO_2/Si where the film is *c*-axis oriented but there is no in-plane orientational locking.

Figure 16 shows the effect of these grain boundaries on the low-field magnetotransport properties, at a temperature (77 K) well below the Curie temperature or the maximum resistance temperature. The epitaxial film shows almost no MR; however, the films with grain boundaries show a much larger, negative magnetoresistance compared to the epitaxial films. This is one of the interesting aspects of transport in these

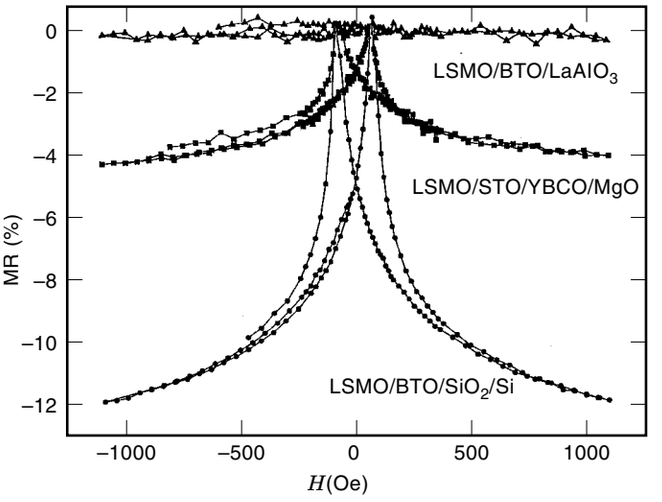

Figure 16. Low-field MR for the three types of films described in Fig. 14, illustrating the beneficial effects of the in-plane grain boundaries.

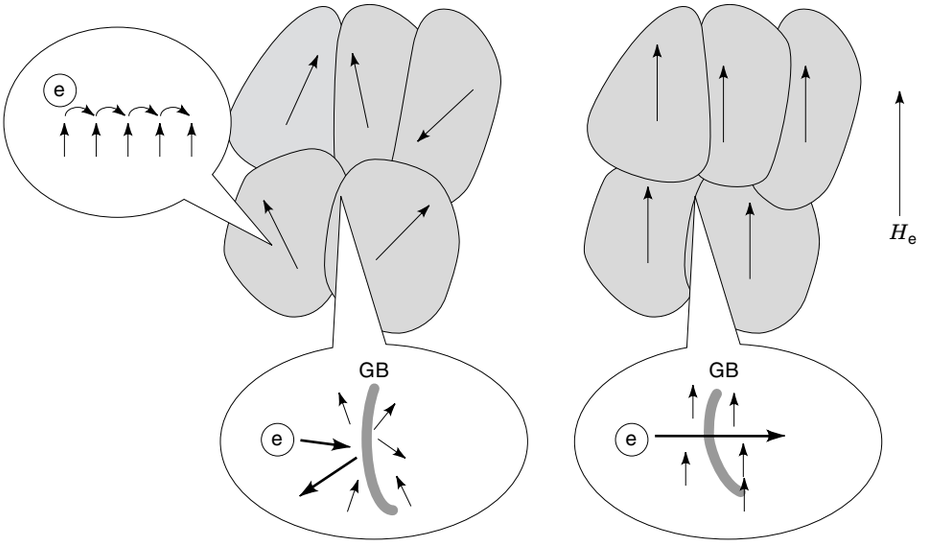

Figure 17. A schematic illustration of the possible mechanism by which the large MR effects are observed in the granular films. At zero field, the magnetization vectors in each grain is randomly oriented in addition to the intrinsic spin disorder at the grain boundaries; when a field is applied the spins within the grains reorient and thus reduce the scattering within the grain, leading to a lower resistance.

materials that still needs detailed elucidation. Figure 17 shows schematically a possible model to explain the large field-dependent MR in the films with grain boundaries. We suspect that the intrinsic structural disorder at the grain boundaries (the degree of which depends on the nature of the grain boundary, namely whether it is a CSL-type semicoherent grain boundary or a fully random grain boundary) leads to spin disorder very close to the grain boundaries. Upon application of a small magnetic field, the ferromagnetic material inside the grain becomes fully magnetized while the grain boundary regions are still not fully aligned in the applied field direction (15). The effective field at the grain boundaries is of the order of $H_e + 4\pi M$, and even though the external field H_e is only a few hundred Oersteds, the total field is of the order of a few thousand Oersteds. It is still unclear if this effective internal field is sufficient to cause the alignment of spins in the grain boundary regions, and further systematic studies are required.

A second approach to low-field MR in these oxides is through heterostructuring. Two types of heterostructure devices, namely spin valves (16–18) and spin tunnel devices, are being explored in many laboratories. A typical example of a spin valve is shown schematically in Fig. 18. Such a device typically consists of two ferromagnetic (FM) layers (significantly different coercive fields) separated by a metallic, nonferromagnetic layer. Case 1 in this figure shows the condition where the two FM layers are polarized in the same direction. Under these conditions, if a spin-polarized electron is launched from the bottom FM layer, then it can pass into the upper FM layer through the normal metal layer without any hinderance leading to a low resistance. However, if Case 2 is true, the spin-polarized electron launched from the bottom FM layer will get scattered at the upper FM/metal interface, and the resistance will be higher. In some sense, these two different resistance values correspond to two different logic states (as in a memory element). Control of the spin orientation is through the coercive fields of the two layers. Typically, one of the layers has a much higher coercive field or is pinned to one magnetization state by exchange biasing through a layer underneath. This is illustrated in Fig. 19 through schematic hysteresis loops. The hysteresis loop in the bottom of this figure shows the characteristic split indicative of the two distinctly different coercive fields. The corresponding MR plot is shown in Fig. 20. Large values of spin-dependent MR values are obtained in the intermediate field regime where the spins in the two FM layers are antiparallel.

Using these concepts, we have been exploring approaches to obtain large MR values in heterostructures that use the CMR perovskites as one of the FM layers, as schematically illustrated in Fig. 21. The intrinsic similarity in crystal structure and chemistry between these materials (i.e., they are all based on oxygen octahedra) means that heteroepitaxy is feasible. Indeed, X-ray diffraction patterns from prototypical het-

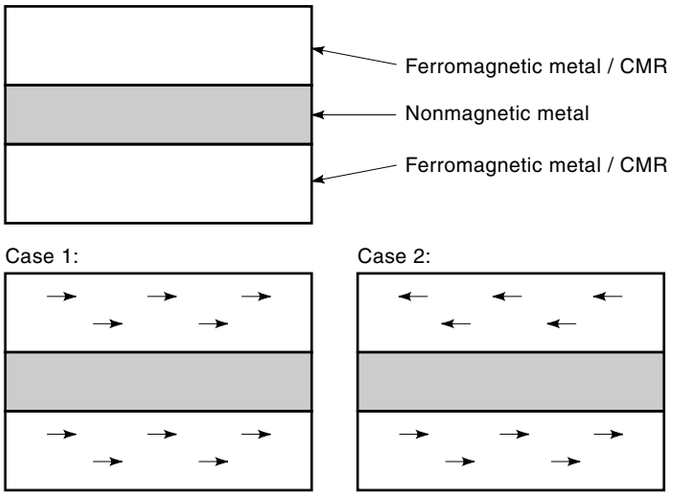

Figure 18. A schematic illustration of the trilayer structure of a spin valve illustrating the origin of scattering that is dependent on the relative orientations of the spin polarizations in the two FM layers.

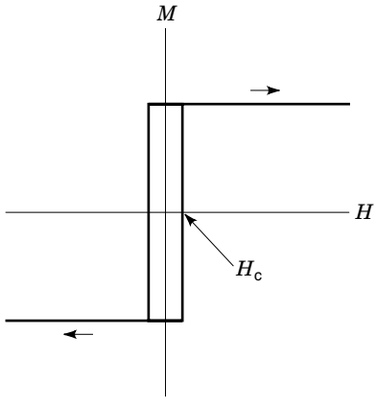

H_c is a parameter of the material that is controlled by the composition of the material and the preparation of the material.

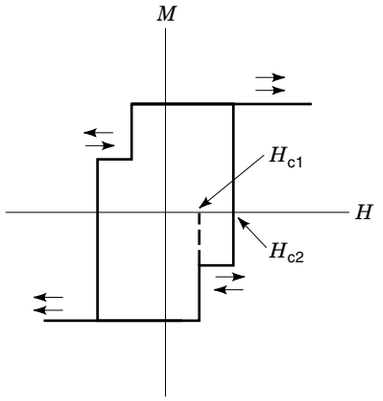

R_J is related to the relative spin orientation, and the relative spin orientation depends on the magnetic field, so $R_J = R_J(H)$.

Figure 19. A schematic diagram of the method by which the spin polarizations in the two layers are controlled through the coercivities of the two FM layers.

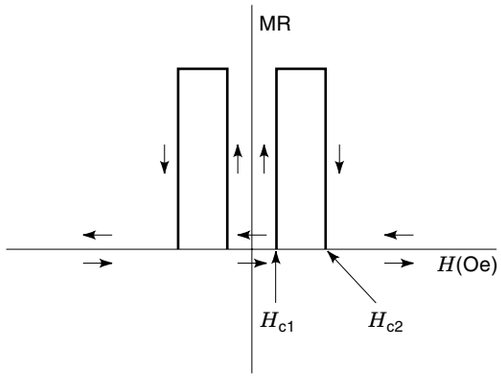

Figure 20. The MR corresponding to the hysteresis loop shown in Fig. 19 for the spin valve illustrated in Fig. 18.

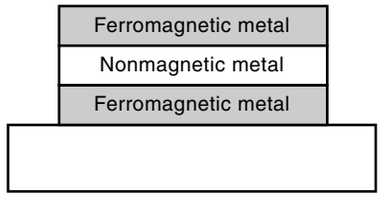

Ferromagnetic metal: LSMO
LBMO
Fe_3O_4

Nonmagnetic metal: $La_{0.5}Sr_{0.5}CoO_3$
$SrRuO_3$

Figure 21. A schematic diagram of the all-oxide spin valve that is being explored in our program.

erostructures grown using LSMO as the FM top and bottom layers and LSCO as the nonferromagnetic metallic layer show excellent in-plane as well as out-of-plane structural coherence. Ferromagnetic hysteresis loops obtained from these heterostructures show clear proof of the existence of two distinct coercive fields (Fig. 22), which is one prime requirement for a spin valve to operate. Transport measurements are currently under way, and the details of magnetotransport in these spin valves should become clearer over the next year.

CONCLUDING REMARKS

Colossal magnetoresistance in perovskite manganates is not a new phenomenon in the same way that the materials themselves are not new. What has happened over the past few years is that new materials processing approaches and the knowledge that has been obtained from the high-temperature superconductivity research arena have transferred over to magnetic oxides. For example, the ability to grow epitaxial perovskites has been and continues to be an important prerequisite to the explosion of research in the CMR area. Although it appears doubtful that large MR values will be obtained at low magnetic fields in single thin-film layers of the CMR perovskites, the recent results of magnetotransport measurements in polycrystalline films appear to be very

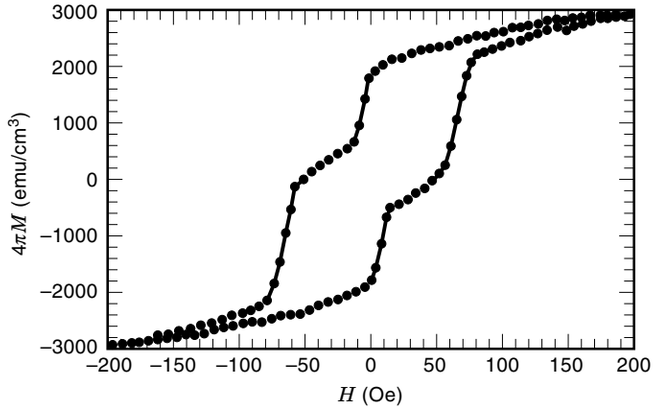

Figure 22. Magnetic hysteresis loop of a LSMO/LSCO/LSMO trilayer spin valve showing the two distinct coercive fields that are a basic requirement for a spin valve operation.

promising in this regard. More detailed studies are required to understand the origins of the behavior and to see if large MR values can be obtained at room temperature and low fields. What has become more exciting is the natural evolution to multilayered heterostructures, such as the spin valve or the spin tunnel junctions. The next few years should bring considerable excitement to this area of research.

BIBLIOGRAPHY

1. J. Goodenough, *Prog. Solid State Chem.,* **5**: 145, 1972.
2. K. Chahara et al., *Appl. Phys. Lett.,* **63**: 1990, 1993.
3. R. Von Helmholt et al., *Phys. Rev. Lett.,* **71**: 2331, 1993.
4. S. Jin et al., *Science,* **264**: 413, 1994.
5. G C. Xiaong et al., *Appl. Phys. Lett.,* **66**: 1427, 1995.
6. C. Kwon et al., *J. Magn. Mag. Matls.,* in press.
7. S. Kaplan et al., *Phys. Rev. Lett.,* **77**: 2081, 1996.
8. K. Ghosh et al., *Phys. Rev. B, Condens. Matter,* in press.
9. H. Y. Hwang et al., *Phys. Rev. Lett.,* **77**: 2041, 1996.
10. H. L. Ju et al., *Phys. Rev. B, Condens. Matter,* **51**: 6143, 1995.
11. A. Gupta et al., *Phys. Rev. B, Condens. Matter,* **54**: 15629, 1996.
12. Y. Lu et al., *Phys. Rev. B, Condens. Matter,* **54**: 8357, 1996.
13. J. Z. Sun et al., *Appl. Phys. Lett.,* **69**: 3266, 1996.
14. T. S. Ravi et al., *Phys. Rev. B, Condens. Matter,* **42**: 10141, 1990.
15. N. D. Mathur et al., *Nature,* in press.
16. M. Johnson and R. H. Silsbee, Interfacial charge-spin coupling: Injection and detection of spin magnetization in metals, *Phys. Rev. Lett.,* **55**: 1790, 1985.
17. M. Johnson, Bipolar spin switch, *Science,* **260**: 320, 1993.
18. M. Johnson, The all-metal spin transistor, *IEEE Spectrum,* **31**: 47, 1994.

R. RAMESH
T. VENKATESAN
University of Maryland

MAGNETORESISTANCE, THERMAL. See THERMAL MAGNETORESISTANCE.